# Fiber-delivered heterodyne spectroscopy with a mid-infrared frequency comb

PABLO CASTRO-MARIN,<sup>1</sup> © KERR JOHNSON,<sup>2</sup> © CARL FARRELL,<sup>2</sup> IAN A. DAVIDSON,<sup>3</sup> © QIANG FU,<sup>3</sup> © GREGORY T. JASION,<sup>3</sup> © NATALIE V. WHEELER,<sup>3</sup> FRANCESCO POLETTI,<sup>3</sup> DAVID J. RICHARDSON,<sup>3</sup> AND DERRYCK T. REID<sup>1,\*</sup> ©

**Abstract:** By exploiting the excellent short-term phase stability between consecutive pulses from a free-running optical parametric oscillator frequency comb, we report the first example of hollow-core fiber-delivered heterodyne spectroscopy in the  $3.1–3.8~\mu m$  wavelength range. The technique provides a means of spectroscopically interrogating a sample situated at the distal end of a fiber, with all electronics and light sources situated at the proximal end and with an inherent capability to suppress spectroscopically interfering features present in the free-space and in-fiber delivery path. Using a silica anti-resonant, hollow-core delivery fiber, we demonstrate high quality transmission and attenuated total reflectance spectroscopy of a plastic sample for fiber lengths of up to 40~m, significantly exceeding the few-meter lengths typically possible using solid-core fibers. The technique opens a route to implementing multi-species spectroscopic monitoring in remote and / or hostile industrial environments and medical applications.

Published by Optica Publishing Group under the terms of the Creative Commons Attribution 4.0 License. Further distribution of this work must maintain attribution to the author(s) and the published article's title, journal citation, and DOI.

#### 1. Introduction

Mid-infrared (mid-IR) spectroscopy in the 3–5  $\mu$ m fingerprint band can address diverse chemical sensing applications in industry and medicine [1], which fiber-delivery has the potential to extend to inaccessible or hazardous environments. Conventional single-mode mid-IR fibers based on fluoride and chalcogenide glass are fragile and available commercially in lengths of only a few meters. By contrast, new silica anti-resonant hollow-core fibers (HCFs) offer low-loss waveguiding beyond the transmission-wavelength cut-off of silica (due to guidance in the hollow-core), while 1550-nm and mid-IR guiding HCF designs having already been drawn to 10 km and >100 m length scales respectively [2,3], with further increases in mid-IR yield readily achievable. Low-loss mid-IR HCFs have been reported [4,5], with losses as low as 18 dB km<sup>-1</sup> at 3.1  $\mu$ m recently being achieved [6].

Recently, we reported implementations of remote multi-species fiber-delivered mid-IR spectroscopy in solid-core  $ZrF_4$  fiber [7] and hollow-core silica fiber up to a distance of 63 m [8]. In each example, a homodyne form of Fourier-transform spectroscopy was used, in which light from a broadband source was modulated by a scanning Michelson interferometer before being launched into the fiber and subsequently detected by a photodetector located at the fiber's distal end. Homodyne methods such as this [9,10] impose no requirements on the temporal coherence of the source, because the interference signal is recorded about an optical path difference of zero, allowing thermal emitters and incoherent supercontinuum sources [11] to be readily exploited.

<sup>&</sup>lt;sup>1</sup>School of Engineering and Physical Sciences, Heriot-Watt University, Edinburgh, EH14 4AS, UK <sup>2</sup>Chromacity Ltd, Livingstone House, 43 Discovery Terrace, Research Avenue North, Riccarton, Edinburgh, EH14 4AP, UK

<sup>&</sup>lt;sup>3</sup> Optoelectronics Research Centre, Zepler Institute, University of Southampton, Southampton, SO17 1BJ, UK

<sup>\*</sup>D.T.Reid@hw.ac.uk

Here we report an alternative approach based on heterodyne spectroscopy using a free-running mid-infrared frequency comb, which solves important practical issues facing fiber-delivered remote spectroscopy, including how to detect the spectroscopic signal and how to mitigate the impact of parasitic absorptions in the delivery channel.

# 2. Heterodyne Fourier-transform spectroscopy using an optical parametric oscillator frequency comb

Contrary to homodyne implementations in which the sample and interferometer are separated, in heterodyne Fourier-transform spectroscopy the sample resides in one arm of an imbalanced Michelson interferometer. Coherent heterodyne detection has already been applied in dual-comb spectroscopy, where asynchronous pulses from two mutually-coherent frequency combs are used, one to probe the sample in transmission and the other as a local oscillator to coherently gate the transmitted pulses, providing both phase and amplitude information [12,13,14,15]. Early work on the phase control of ultrashort light pulses demonstrated the phase stability between successive pulses from a free-running Ti:sapphire laser comb [16] and concluded that (for this particular laser) mutual coherence was maintained across approximately 1,000 consecutive pulses. These insights suggest that a free-running mid-infrared frequency comb should permit heterodyne spectroscopy in a Michelson configuration with considerably different arm lengths, potentially enabling remote sensing over hundreds of meters.

Figure 1 illustrates the concept of fiber-delivered mid-infrared heterodyne spectroscopy, where the delivery fiber forms one arm of a Michelson interferometer. When the difference between the physical arm lengths satisfies  $|L_1 - L_2| = mc/2f_{rep}$ , the  $m^{th}$ -neighbor local-oscillator pulses from Arm 2 can coherently gate the pulses returned from the reflectors after the fiber in Arm 1. The transmission spectroscopy of the sample is obtained from the ratio of the spectra of the two interferograms, which are isolated in respective delay windows that allow their Fourier transforms to be performed for this purpose. The apparatus can be adapted to enable attenuated total reflectance (ATR) spectroscopy, a contact technique applicable to most solids and liquids and characterized by high reproducibility and minimal sample preparation. As shown in Fig. 1 (inset), a ZnSe right-angled prism can be introduced into the collimated output beam from the HCF. The light enters through one of the two shorter faces of the prism, from which a reference interferogram is obtained from the Fresnel reflection. After interacting with the sample through the evanescent field present at the interface, light is reflected from the other shorter face and returned, via the HCF, to the detector to yield the sample interferogram.

The heterodyne approach possesses several characteristics which make it attractive for remote fiber sensing. The reference spectrum obtained from the reflector immediately after the fiber output allows all spectroscopic features present on the light up to this point to be measured, and to be subsequently removed from the sample spectroscopy, providing strong common-mode rejection of even narrow features like gas absorption lines present in the fiber delivery channel. Similarly, because the measurement is a ratio, it is independent of the spectral intensity profile of the light source, meaning that drift and instability in the source spectrum have little impact on the spectroscopy. Where the reference and sample reflectors are opposite ends of a gas cell, the interferogram delay positions automatically provide the length of the transmission path inside the cell, enabling the path-integrated concentration to be accurately determined. Finally, by retaining all the detection apparatus at the proximal end of the fiber, no photodetectors or other electronics are needed at the distal end, meaning that sensing in electromagnetically sensitive or explosive environments is possible.

In the remainder of this article we describe three experimental implementations of fiber-delivered heterodyne spectroscopy using light in the 3.1–3.8 µm wavelength range delivered through silica HCF. First, we demonstrate the technique in a simple transmission mode using 3.6 m of HCF delivery fiber, illustrating the strong common-mode rejection of features such as

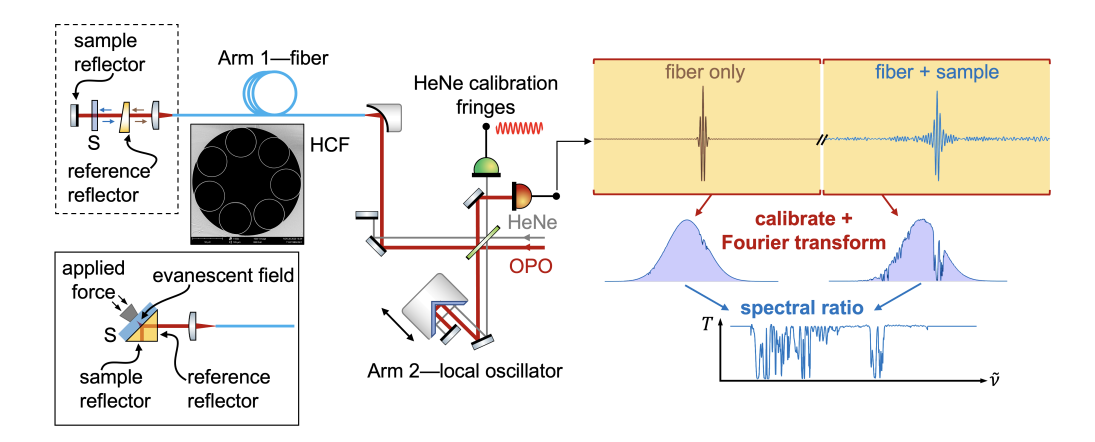


**Fig. 1.** Concept of fiber-delivered heterodyne spectroscopy. Light from a mid-IR broadband OPO frequency comb is launched into a hollow-core fiber (Arm 1) using an off-axis parabolic mirror and returned by reflections from a ZnSe reference wedge and a metal mirror situated after a thin plastic sample (S). Coherent gating with subsequent pulses from the OPO (Arm 2) results in interferograms, whose Fourier transforms yield the spectra of the fiber alone (reference reflector) and of the fiber and sample combined (metal mirror). The spectral ratio of these provides the double-pass sample transmission spectrum. Inset: Optics for ATR spectroscopy, replacing those in the dashed box.

etalons or gas absorption lines that are written onto the light as it propagates to the sample from the OPO and through the delivery fiber. Next, using the same sample, we show the system's adaptation to an ATR spectroscopy mode. Finally, we present results exploring the performance limitations of the technique when using a 40-meter-long HCF, considerably longer than is possible using conventional fluoride or soft-glass delivery fibers.

### 3. Implementation of fiber-delivered heterodyne spectroscopy

#### 3.1. Transmission spectroscopy with a 3.6-meter-long HCF delivery fiber

The experimental layout closely followed the schematic in Fig. 1. The light source was a commercial ultrafast optical parametric oscillator (OPO) from Chromacity Ltd. similar to that described previously [7,10]. The OPO produced >150-fs idler pulses at a 100-MHz repetition rate, which had a typical instantaneous bandwidth of around 200 nm and produced an average power of up to 300 mW. The center wavelength of the OPO was tunable from 2.9–3.8 µm (2630–3450 cm<sup>-1</sup>), enabling spectroscopy across this region. Light from the OPO was divided equally between Arm 1 and Arm 2 using a non-polarizing 50:50 beamsplitter. The delay in Arm 2 was scanned at 1 Hz using a retroreflector mounted on an electromagnetic linear actuator with a range of up to 80 mm. A co-propagating beam from a linearly polarized HeNe laser provided a fringe sequence that was used to precisely calibrate the movement of the retroreflector. Light returned from Arm 2 was incident on a InAsSb amplified detector (Thorlabs, PDA10PT) and provided the local oscillator pulses for the measurement.

Light entering Arm 1 was launched with 60% coupling efficiency into anti-resonant HCF using an off-axis parabolic reflector. The anti-resonant HCF had a core diameter of 77  $\mu$ m, cladding tubes of average diameter 51  $\mu$ m, an average inter-tube gap of 5.2  $\mu$ m, and tube-membrane thicknesses of ~930 nm [8]. A Fresnel reflection from a CaF<sub>2</sub> wedge located after the end of the fiber returned a percentage of the light to serve as the reference spectrum, with the remainder transiting a free-space section before being returned by another reflection from a partial reflector.

Spectroscopy was performed by introducing a thin polystyrene-film sample into this free-space region. After a further transit through the fiber, these reflections were gated by the pulses from Arm 2 to produce interferograms from the reference and sample reflections.

The resulting interferograms were acquired, together with the HeNe fringes, using an ADLINK PCI-9816 H digitizer operating at a sampling rate of 10 MSa/s and with 16-bit resolution. For a fiber length of 3.6 m, the interferograms resulted from interference between the second-neighbor (m=2) pulses from Arms 1 and 2. After first using the HeNe fringes to calibrate the delay scale of the mid-IR signal, the sample and reference interferograms were extracted using two non-overlapping Norton-Beer apodization windows of equal widths and each centered on the peak of their respective interferogram. The spectroscopic resolution provided by the windowing procedure was  $0.14 \, \mathrm{cm}^{-1}$  and this equal treatment of both interferograms ensured that narrow common-mode features such as gas absorption lines were broadened equally by the instrument function and so were strongly suppressed when the spectral ratio was calculated.

Calibrating the instrument involves measuring reference and sample spectra with no sample present to obtain an instrument response factor,  $\rho_o(\omega)$  (see Appendix). Shown in Figs. 2(a) and 2(b), the measurements (solid lines) are composites of spectra recorded at eleven different OPO tuning positions from 2600-3200 cm<sup>-1</sup>, with each constituent spectrum being the average of 32 individual spectra. The power incident on the InAsSb detector was 1.5 mW from Arm 1 and 1.8 mW from Arm 2 (the local oscillator). The standard deviation of the composite spectrum is shown by the blue shading  $(\pm 1\sigma)$ . The spectral features observed are characteristic of those added by etalons and gas absorption lines in the free-space and in-fiber sections of the optical path to the sample. In addition to naturally occurring atmospheric species like CH<sub>4</sub> and H<sub>2</sub>O, inside the fiber there is also HCl present from the fabrication process. The calculated instrument response factor,  $\rho_o(\omega)$ , is shown in Fig. 2(c) and is almost spectrally flat. Notably, the contributions to the transmission spectrum of etalon modulation and molecular absorption features are nearly entirely absent, illustrating the powerful common-mode rejection provided by the heterodyne measurement, which otherwise could only be mitigated by purging the fiber [3]. Before using  $\rho_o(\omega)$  to correct subsequent measurements (see Appendix), we applied a Savitzky-Golay (SG) fit (Fig. 2(c), red line) to eliminate any residual fine spectral structure while still retaining the broad spectral variations.

Spectroscopy was evaluated using a calibrated plastic sample of polystyrene film (PS; 35 µm thick). Separate reference, sample and calculated transmission spectra are shown in Figs. 2(d), 2(e) and 2(f). For comparison, an independently measured library spectrum is shown in red. Our measurement corresponds closely to the library spectrum, which originates from a database providing both FTIR transmission and ATR measurements [17].

#### 3.2. Fibre-delivered attenuated total reflectance spectroscopy

As described earlier, heterodyne spectroscopy eliminates the need for any detection electronics at the distal end of the fiber. When combined with ATR spectroscopy [18], it therefore presents the opportunity for a simple fiber-delivered spectroscopic contact probe. Here, we describe the extension of the transmission mode to an ATR spectroscopy embodiment using a 3.6-m-long HCF delivery fiber.

We implemented ATR spectroscopy using an uncoated ZnSe right-angled isosceles prism (Thorlabs PS701). The high refractive index of ZnSe (n = 2.43 at a wavelength of 3.3 µm [19]) provides a Fresnel reflection at normal incidence of 17%. As illustrated in Fig. 1, collimated light from the distal end of the fiber entered the prism through one of the shorter faces, with the Fresnel reflection from this face providing the reference reflection. After total internal reflection at the prism hypotenuse (the ATR sensing surface), an internal Fresnel reflection from the other shorter prism face provided the sample reflection. Similar to the signal obtained in the transmission spectroscopy mode, the ATR signal comprised two interferograms, whose Fourier transforms

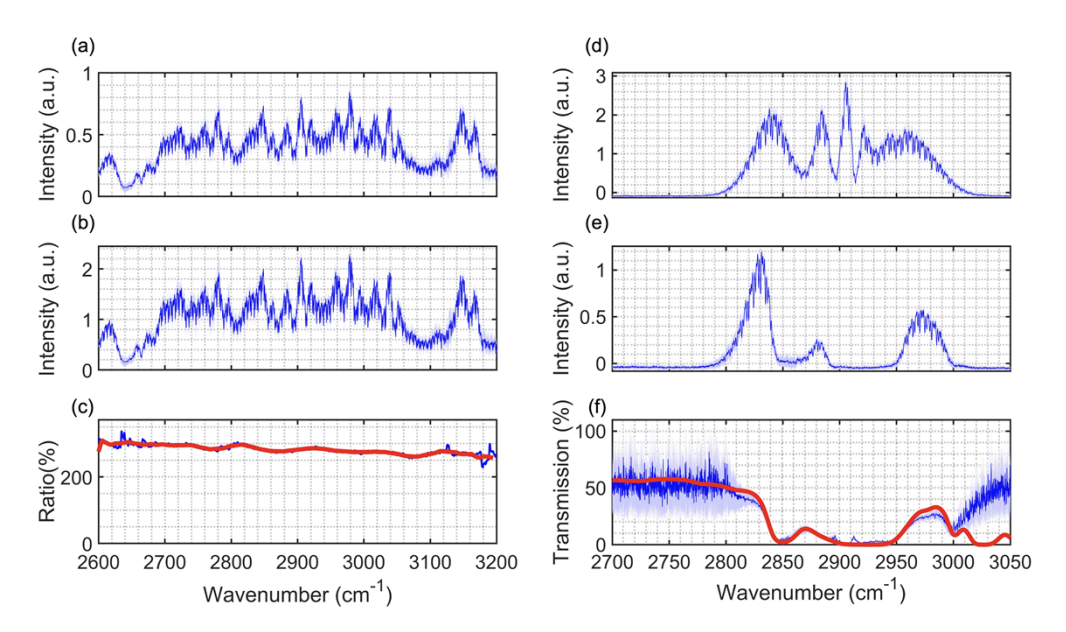


**Fig. 2.** Transmission spectroscopy using a 3.6 m HCF delivery fiber. (a) Reference spectrum, (b) sample spectrum, and (c) instrument response spectrum  $\rho_o(\omega)$  shown in blue and fitted (red) with a Savitzky-Golay polynomial filter. (d) Reference spectrum, (e) sample spectrum with polystyrene film, and (f) calculated transmission of the polystyrene film, co-plotted with library data (red) having a resolution of  $8 \, \mathrm{cm}^{-1}$  [17].

provided the spectra of the reference and sample reflections. The prism size determines the delay interval separating these interferograms, in turn limiting the apodization window which can be applied, and ultimately the spectral resolution. The prism we used had shorter faces with lengths of 10 mm, implying a reference-signal interferogram separation of 160 ps, and leading to a spectral resolution of  $0.2 \, \mathrm{cm}^{-1}$ . This resolution is more than sufficient to resolve the spectroscopic features present in the solid and liquid samples typically analyzed using ATR spectroscopy.

To achieve a strong ATR signal we developed a custom prism holder that included a small clamp, enabling us to apply pressure to the sample and so improve its contact with the prism face and the evanescent field, a well-known requirement in ATR spectroscopy [20]. Figure 3 shows the 3D-printed prism holder and clamp designed for this purpose.

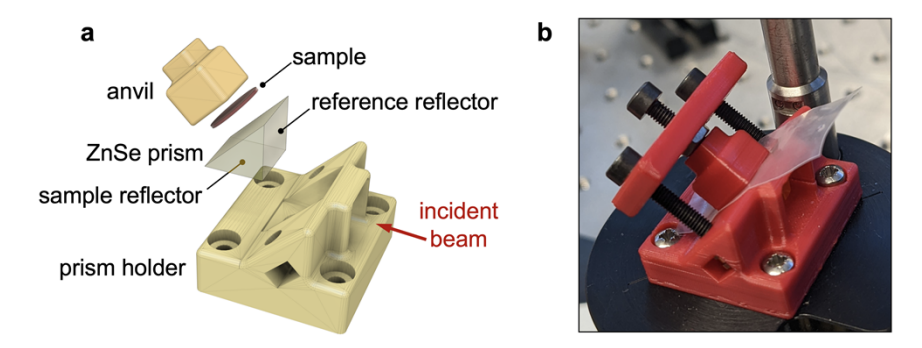


**Fig. 3.** (a) Design and (b) 3D-printed realization of a prism holder and clamp arrangement to achieve a strong ATR signal.

As described in Section 3.1, we recorded the instrument function from the system with no sample in contact with the prism, aligning the prism to provide reference and sample interferograms of comparable amplitudes. The resulting spectra are shown in Figs. 4(a) and 4(b), with the calculated response function,  $\rho_o(\omega)$ , shown in Fig. 4(c). We believe the slope observed in  $\rho_o(\omega)$  results from chromatic aberration in the collimation lens after the HCF, which introduces a spatial dependence in the spectrum. When both the reference and sample reflectors can be independently optimized for normal incidence this effect can be mitigated (for example, in the embodiment described in Section 3.1), but this is not possible with a prism in which the reflecting faces are rigidly coupled and may not be at exactly 90° to one another. The measured  $\rho_o(\omega)$  was used to correct for this wavelength-dependent bias in subsequent spectroscopy measurements (Appendix, Eq. (10)). Figures 4(d) and 4(e) show the measured reference and sample spectra when the same polystyrene sample used in the transmission spectroscopy measurements was brought into contact with the prism ATR face. The calculated transmission spectrum is shown in Fig. 4(f) and corresponds well with library ATR spectroscopy data for polystyrene (Fig. 4(f), red). We note that the relative band strengths and positions determined by ATR spectroscopy depend on the applied force [20], therefore an exact overlap between the library data and experiment is not expected.

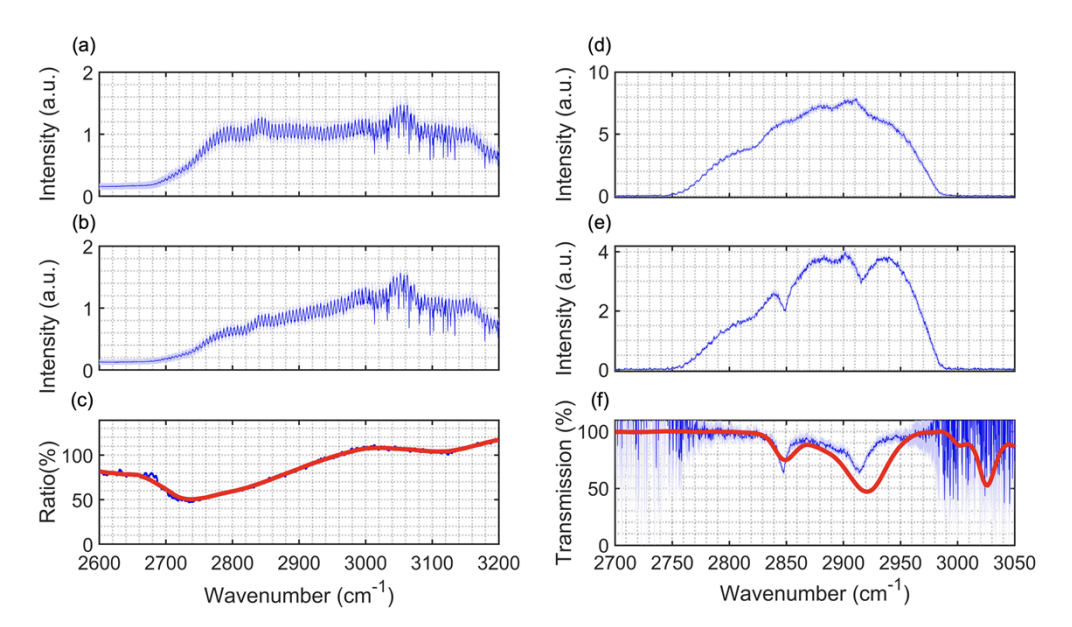


**Fig. 4.** ATR spectroscopy using a 3.6 m HCF delivery fiber. (a) Reference and (b) sample spectra for no sample in contact with the prism. (c) Calculated instrument response function and its SG polynomial fit (red). (d) Reference spectrum and (e) sample spectrum with a polystyrene film in contact with the prism. (f) Calculated transmission of the polystyrene film and its comparison with library data (red) having a resolution of  $4\,\mathrm{cm}^{-1}$  [17].

## 3.3. Transmission spectroscopy with a 40-meter-long HCF delivery fiber

The robust material properties and relatively low mid-IR loss of silica HCF enable transmission over considerably longer lengths than can be achieved using conventional fluoride and soft-glass fibers. Previously, we reported gas spectroscopy after single-pass transmission through 63 m of HCF [8]. Here, we describe heterodyne transmission spectroscopy measurements after 40 m of HCF, involving a double-pass through the fiber and a total in-fiber path of 80 m. In comparison to shorter fiber length used for the measurements described in Section 3.1, there is considerably

greater spectral interference from water vapor, HCl, and methane trapped inside the fiber core. Consequently, measurements in a 40-m-long fiber present a challenging test of the common-mode rejection capability inherent in the heterodyne measurement.

In [8] we reported a minimum loss of around  $0.15\,dB~m^{-1}$  in the spectral region from  $3.2\text{--}3.5~\mu m$ , implying around 6% transmission before coupling losses are taken into consideration. For this reason we modified the arrangement in Section 3.1~by using optics with higher reflectivities for the reference and sample reflectors. The  $CaF_2$  wedge was changed for a Ge wedge, and a silver mirror was used after the sample. In this configuration, the power from Arm 1 reaching the photodetector was  $\approx 1~mW$  and we used the detector in a high-gain mode while also limiting the local-oscillator power.

Figure 5 presents the results obtained, following a similar format to previously. The reference and sample calibration spectra shown, respectively, in Figs. 5(a) and 5(b) display severe spectral structure, mainly from water vapor and HCl. The ratio shown in Fig. 5(c) exhibits some associated structure, resulting from the sensitivity of ratioing steep features at the edges of the HCl absorption lines. After applying a Savitzky-Golay fit the instrument function becomes smooth and uniform (Fig. 5(c), red), allowing it to be used for spectral baseline correction in the measurements shown in Figs. 5(d) to 5(f). To allow comparison with earlier measurements, we again used a thin polystyrene film as the spectroscopy sample, and Fig. 5(f) shows the resulting transmission obtained, and its correspondence with library data measured with the considerably lower spectral resolution of 8 cm<sup>-1</sup> (red). The agreement is generally good, with the exception of the presence of sharp spectral artefacts associated with small line-shape differences that prevent complete common-mode rejection when calculating the ratio of the reference and sample spectra. These artefacts are very sharp and are associated with negligible spectral power.

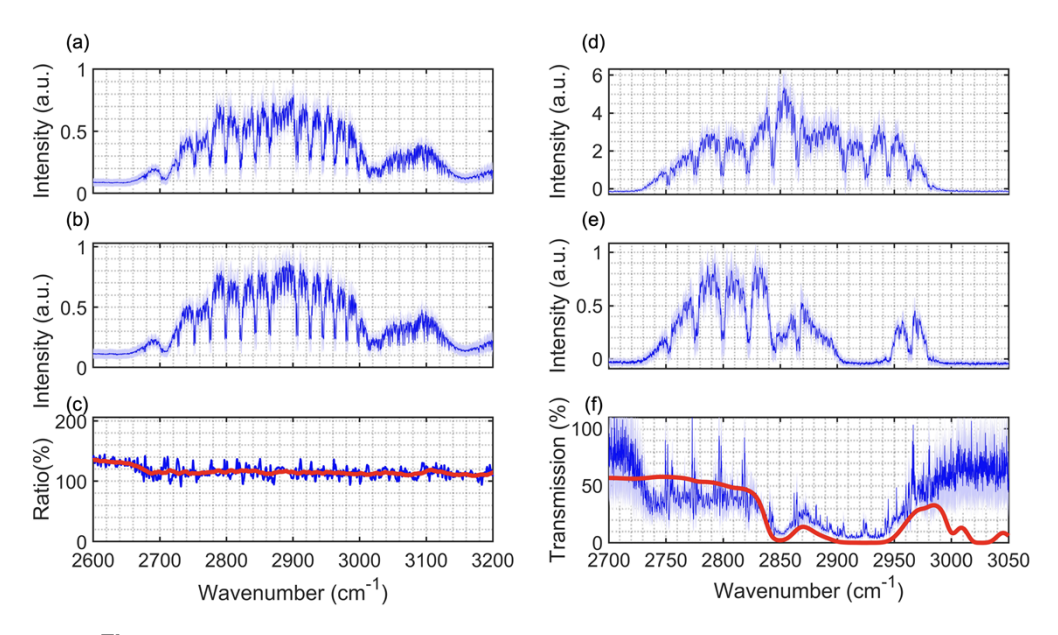


**Fig. 5.** Transmission spectroscopy using a 40 m HCF delivery fiber. (a) Reference spectrum, (b) sample spectrum, and (c) instrument response spectrum  $\rho_o(\omega)$  shown in blue and fitted (red) with a Savitzky-Golay polynomial filter. (d) Reference spectrum, (e) sample spectrum with polystyrene film, and (f) calculated transmission of the polystyrene film, co-plotted with library data (red) having a resolution of  $8 \text{ cm}^{-1}$  [17].

#### 4. Conclusions

We have introduced here a new modality, fiber-delivered heterodyne spectroscopy, which is uniquely enabled by the long-term temporal coherence that exists across a series of ultrafast pulses from a mid-infrared frequency comb source. While ruling out thermal, super-luminescence and incoherent supercontinuum sources, the constraints on the comb properties are otherwise not severe. No repetition-rate stabilization is required, since the typical pulse-to-pulse free-running timing jitter is still much less than the carrier period of mid-infrared light. Similarly, the carrier-envelope phase of free-running OPOs is sufficiently stable to allow coherence over many microseconds, with the potential to observe interference between pulses separated by hundreds of roundtrips.

By using a normal-incidence Fresnel reflection after the delivery fiber but before the sample, we can access a near-ideal spectroscopic baseline measurement that allows us to treat spectrally interfering features in the delivery path (both free-space and in-fiber) as an instrument response function, which can be corrected for in subsequent spectroscopy.

The results presented here exclusively used hollow-core fiber, which benefits from very low group-delay dispersion, ensuring that the interferograms can be confined to a delay range determined only by the desired spectroscopy resolution, rather than by dispersive pulse broadening, which for commercially available mid-IR fibers at 3.3 µm is around 2 ps per meter for the spectral bandwidths reported here [21].

In the demonstrated system, the length of the delivery fiber must be carefully chosen to ensure the local-oscillator and spectroscopy pulses coincide at the detector around the center of the delay-stage scan; however, this is generally not a limitation since any fiber length can be compensated for with a fixed delay in the local-oscillator arm. Furthermore, because both interferograms are measured by the same detector, it is important to arrange the reflectivities of the reference and sample reflectors to equalize the amplitudes of the corresponding interferograms. Doing so maximizes the dynamic range available from the digitizer and mitigates any nonlinear response present.

Because no electronics, light sources, or electrical power are needed at the distal end of the fiber, HCF-delivered heterodyne spectroscopy opens a route to implementing multi-species spectroscopic monitoring in remote, explosive or otherwise hostile industrial environments and medical applications. Purging the core of the HCF with dry air or nitrogen would eliminate the most intense spectral interference and would further improve the performance of the technique over the longest fiber lengths.

#### Appendix: Calculation of the sample transmission

The interferogram produced by a delay-scanning heterodyne Michelson interferometer is:

$$\int_{-\infty}^{\infty} |E_{S(R)}(t) + E_{LO}(t - \tau)|^2 dt \tag{1}$$

where  $E_{LO}$  is the field of the local-oscillator pulses,  $E_R$  the field of the pulses returned to the beamsplitter by the reference reflector, and  $E_S$  the field of the pulses returned by the reflector after the sample.

The interferogram can be expanded as,

$$\int_{-\infty}^{\infty} [E_{S(R)}(t) + E_{LO}(t-\tau)] [E_{S(R)}(t) + E_{LO}(t-\tau)]^* dt, \tag{2}$$

which comprises constant terms proportional to the power from the individual interferometer arms, together with the interference term and its complex conjugate (c.c.),

$$I_{S(R)}(\tau) = \int_{-\infty}^{\infty} E_{S(R)}(t) E_{LO}^*(t-\tau) dt + c.c.$$
 (3a)

$$= E_{S(R)}(t) \otimes E_{LO}^*(-t) + c.c.$$
 (3b)

$$= \mathcal{F}^{-1} \{ e_{S(R)}(\omega) e_{LO}^*(\omega) \} + c.c.$$
 (3c)

where  $e(\omega) = \mathcal{F}\{E(t)\}\$ and  $e^*(\omega) = \mathcal{F}\{E^*(-t)\}.$ 

Fourier transforming the interferogram yields the power spectrum and its conjugate:

$$S_{S(R)}(\omega) = e_{S(R)}(\omega)e_{LO}^*(\omega) = \mathcal{F}\{I_{S(R)}(\tau)\}. \tag{4}$$

Separately apodizing and Fourier transforming the reference and sample interferogram signals,  $I_R(\tau)$  and  $I_S(\tau)$  respectively, yields reference and sample spectra:

$$S_R(\omega) = e_R(\omega)e_{LO}^*(\omega) \tag{5a}$$

$$S_S(\omega) = e_S(\omega)e_{IO}^*(\omega), \tag{5b}$$

The total transmission path common to both the reference and sample pulses contributes an absorbance of  $\alpha_T(\omega)$ , while the sample pulses uniquely acquire a double-pass absorbance associated with transmission through the sample,  $2\alpha_S(\omega)$ . Taking also into account the different reflectivities (R) of the reference and sample reflectors, we can write the reference and sample fields as:

$$e_R(\omega) = e_o(\omega) r_R(\omega) \exp[-\alpha_T(\omega)]$$
 (6a)

$$e_S(\omega) = e_O(\omega) r_S(\omega) \exp\left[-\alpha_T(\omega)\right] \exp\left[-2\alpha_S(\omega)\right],$$
 (6b)

The ratio,  $\rho(\omega)$ , of the spectra obtained by Fourier transforming the reference and signal interferograms is:

$$\rho(\omega) = \frac{e_S(\omega)}{e_R(\omega)} = \frac{r_S(\omega)}{r_R(\omega)} \times \exp[-2\alpha_S(\omega)]$$
 (7)

Since we have defined the sample absorbance,  $\alpha_S$ , in terms of field, the sample transmission is  $T(\omega) = \exp[-2\alpha_S(\omega)]$ , and is obtained from the spectral ratio using:

$$T(\omega) = \rho(\omega) \times \frac{r_R(\omega)}{r_S(\omega)}$$
(8)

When the sample is not present, T = 1, so we can use the spectral ratio recorded in this case to provide the calibration factor that accounts for the reflectivities of the reference and sample reflectors:

$$\rho_o(\omega) = \frac{r_S(\omega)}{r_R(\omega)} \tag{9}$$

This sample-free ratio can be considered to be the instrument response function and allows us to express the single-pass sample transmission as the measured spectral ratio corrected by the sample-free spectral ratio:

$$T(\omega) = \rho(\omega)/\rho_o(\omega). \tag{10}$$

**Funding.** Royal Academy of Engineering (RCSRF2223-1678); Royal Society; Engineering and Physical Sciences Research Council (EP/P030181/1); Science and Technology Facilities Council (ST/T000635/1).

**Disclosures.** The authors declare no conflicts of interest.

Data availability. Data supporting the results in this paper may be obtained from the authors on request.

#### References

- 1. J. Hodgkinson and R. P. Tatam, "Optical gas sensing: a review," Meas. Sci. Technol. 24(1), 012004 (2013).
- 2. Y. Chen, Z. Liu, and S. R. Sandoghchi, *et al.*, "Multi-kilometer long, longitudinally uniform hollow core photonic bandgap fibers for broadband low latency data transmission," J. Lightwave Technol. **34**(1), 104–113 (2016).
- 3. Q. Fu, Y. Wu, and I. A. Davidson, *et al.*, "Hundred-meter-scale, kilowatt peak-power, near-diffraction-limited, mid-infrared pulse delivery via the low-loss hollow-core fiber," Opt. Lett. **47**(20), 5301 (2022).
- 4. N. V. Wheeler, A. M. Heidt, and N. K. Baddela, *et al.*, "Low-loss and low-bend-sensitivity mid-infrared guidance in a hollow-core-photonic-bandgap fiber," Opt. Lett. **39**(2), 295–298 (2014).
- 5. I. A. Davidson, OSA conf. on Specialty Optical Fibers (2020) pp. SoW1H-7.
- F. Yu, P. Song, and D. Wu, et al., "Attenuation limit of silica-based hollow-core fiber at mid-IR wavelengths," APL Photonics 4(8), 080803 (2019).
- K. Johnson, P. Castro-Marin, and O. Kara, et al., "High resolution ZrF4-fiber-delivered multi-species infrared spectroscopy," OSA Continuum 3(12), 3595 (2020).
- K. Johnson, P. Castro-Marin, and C. Farrell, et al., "Hollow-core fiber delivery of broadband mid-infrared light for remote spectroscopy," Opt. Express 30(5), 7044 (2022).
- K. A. Tillman, R. R. J. Maier, and D. T. Reid, et al., "Mid-infrared absorption spectroscopy across a 14.4THz spectral range using a broadband femtosecond optical parametric oscillator," Appl. Phys. Lett. 85(16), 3366–3368 (2004).
- O. Kara, F. Sweeney, and M. Rutkauskas, et al., "Open-path multi-species remote sensing with a broadband optical parametric oscillator," Opt. Express 27(15), 21358 (2019).
- K. E. Jahromi, M. Nematollahi, and R. Krebbers, et al., "Fourier transform and grating-based spectroscopy with a mid-infrared supercontinuum source for trace gas detection in fruit quality monitoring," Opt. Express 29(8), 12381 (2021).
- I. Coddington, W. C. Swann, and N. R. Newbury, "Coherent multiheterodyne spectroscopy using stabilized optical frequency combs," Phys. Rev. Lett. 100(1), 013902 (2008).
- I. Coddington, W. C. Swann, and N. R. Newbury, "Coherent dual-comb spectroscopy at high signal-to-noise ratio," Phys. Rev. A 82(4), 043817 (2010).
- I. Coddington, W. C. Swann, and N. R. Newbury, "Time-domain spectroscopy of molecular free-induction decay in the infrared," Opt. Lett. 35(9), 1395–1397 (2010).
- O. Kara, L. Maidment, and T. Gardiner, et al., "Dual-comb spectroscopy in the spectral fingerprint region using OPGaP optical parametric oscillators," Opt. Express 25(26), 32713 (2017).
- L. Xu, T. W. Hänsch, and C. Spielmann, et al., "Route to phase control of ultrashort light pulses," Opt. Lett. 21(24), 2008 (1996).
- S. Primpke, M. Wirth, and C. Lorenz, et al., "Reference database design for the automated analysis of microplastic samples based on Fourier transform infrared (FTIR) spectroscopy," Anal. Bioanal. Chem. 410(21), 5131–5141 (2018).
- 18. M. Milosevic, "Internal reflection and ATR spectroscopy," Appl. Spectrosc. Rev. 39(3), 365-384 (2004).
- 19. D. T. F. Marple, "Refractive index of ZnSe, ZnTe, and CdTe," J. Appl. Phys. 35(3), 539-542 (1964).
- PerkinElmer technical notes for Infrared Spectroscopy, "The effects of varying force and contact on ATR spectra,"
   \$\infty\$2012, https://resources.perkinelmer.com/corporate/cmsresources/images/44-135840tch\_010127\_01\_atr.pdf
- 21. For example, InF3 fiber available from Thorlabs (part number P1-32F) and whose dispersion is reported in R. Salem, Z. Jiang, and D. Liu, *et al.*, "Mid-infrared supercontinuum generation spanning 18 octaves using step-index indium fluoride fiber pumped by a femtosecond fiber laser near 2 μm," Opt. Express **23**(24), 30592 (2015).